Journal of Catalysis **205,** 278–288 (2002)
doi:10.1006/jcat.2001.3452, available online at http://www.idealibrary.com on IDEAL®

Hydrogenation of Crotonaldehyde over Sn/Pt(111) Alloy Model Catalysts

Dmitri I. Jerdev, A. Olivas, and Bruce E. Koel[1]

Department of Chemistry, University of Southern California, Los Angeles, California 90089-0482

Received May 22, 2001; revised September 20, 2001; accepted September 28, 2001

Gas-phase hydrogenation of crotonaldehyde (CH_3CH=$CHCHO$) was studied over the (2 × 2) Sn/Pt(111) and ($\sqrt{3} \times \sqrt{3}$)R30° Sn/Pt(111) surface alloys which were used as model catalysts. The influence of the alloy structure, hydrogen pressure, and temperature on activity and selectivity toward 2-butenol (CH_3CH=$CHCH_2OH$) formation was investigated. The results were compared to those obtained for the pure Pt(111) surface. All catalysts were characterized prior to use by X-ray photoelectron spectroscopy and low-energy electron diffraction to ensure proper alloy formation. The hydrogenation activity was about two times higher for the bimetallic Pt–Sn catalysts compared to that for Pt(111); however, little change in selectivity was observed. Butyraldehyde was formed as the main product in all cases. Therefore, alloy formation improves hydrogenation activity toward C=C and C=O functional groups and cannot solely explain the improvement in selectivity toward the formation of the unsaturated alcohol that has often been reported for supported Pt–Sn catalysts versus pure Pt catalysts. Both alloys investigated had similar catalytic activity and selectivity. An attempt was made to create oxidic tin species on the Pt(111) surface, because these species have been suggested to improve selectivity to the unsaturated alcohol product. However, the oxidic species formed by heating the alloys in 5 Torr O_2 for 5 min at 600 K were not stable under reaction conditions and were reduced to form a surface with low catalytic activity, probably consisting of metallic Sn rafts over the Pt(111) surface.

INTRODUCTION

Pt–Sn bimetallic catalysts are known for their performance and stability in catalytic hydrocarbon transformations. These supported Pt–Sn catalysts have been studied for hydrogenation–dehydrogenation (1), hydrogenolysis (2), and recently for selective oxidation of hydrocarbons (3). In general, Pt bimetallic catalysts exhibit increased stability against coke formation and catalytic behavior different from that of the pure Pt catalysts. Observations that alloys are formed in some catalyst systems and the possibility that alloys are important phases in other systems make alloys interesting targets for investigation.

In this work, we investigated Pt–Sn surface alloys as model, unsupported catalysts for the gas-phase hydrogenation of crotonaldehyde (2-butenal, CH_3CH=$CHCHO$). We compared the activity and selectivity of these alloys to those of similar Pt(111) model catalysts (4) and Pt–Sn supported catalysts studied elsewhere (1). This approach allowed us to address some issues in the mechanism over supported Pt–Sn catalysts that may result from alloy formation. Using these surface alloys instead of supported bimetallic catalysts makes it possible to exclude the influence of several factors, such as metal–support interaction, incomplete reduction of the metal phase(s), size of the active metal particles, and sintering, which are known to strongly affect catalytic behavior (5).

The selective hydrogenation of α,β-unsaturated aldehydes to the corresponding unsaturated alcohols has industrial applications. The alcohols obtained are important intermediates in the production of perfumes, flavorings, and pharmaceuticals. The challenge is to selectively hydrogenate the C=O bond leaving the C=C bond intact. The analysis of thermodynamics shows that hydrogenation of the C=C bond is more favorable than that of C=O hydrogenation, forcing this reaction to be run at low temperatures using kinetic control. However, the addition of hydrogen to the C=C bond occurs faster than that to the C=O bond over all known catalysts for the gas-phase hydrogenation of unsaturated aldehydes (6). Research done using pure metals revealed that the activity rather than the selectivity of the catalyst was more strongly affected by using different metals (6). Most metals hydrogenate both double bonds to some extent, except Pd which is known to be very selective with respect to the C=C bond (7). Currently, the only way to achieve selective hydrogenation to form the unsaturated alcohol with high yield (∼99%) is by reduction using boron or metal hydrides ($NaBH_4$ or $NaAlH_4$) (8). This method is quite valuable in a laboratory but too expensive to carry out on an industrial scale. Therefore, it is of interest to create a selective heterogeneous catalyst that would result in an efficient process for this reaction.

Promoters have been used to improve the selectivity of metal catalysts for the previously mentioned processes. Three groups of promoters are commonly used (9): alkali metal compounds, transition metal compounds, and

[1] To whom correspondence should be addressed. E-mail: koel@chem1.usc.edu.

0021-9517/02 $35.00

nontransition metal additives. The last group has the most prominent effect on catalytic behavior. Because tin belongs to this group and is often involved in a number of bimetallic catalysts, we investigated the influence of alloyed Sn on catalytic hydrogenation of crotonaldehyde over a Pt(111) surface.

EXPERIMENTAL PROCEDURES

All experiments were conducted in the apparatus shown in Fig. 1, which consists of an ultrahigh vacuum (UHV) chamber and an attached, atmospheric pressure batch reactor. The UHV chamber was pumped by an ion pump (240 L/s) and a cryo-pump (1500 L/s) and had a base pressure of 1×10^{-10} Torr. The chamber was equipped with a quadrupole mass spectrometer (QMS) for residual gas analysis and temperature-programmed desorption (TPD), low-energy electron diffraction (LEED) optics, a 180-mm spherical capacitor analyzer (SCA) for Auger electron spectroscopy (AES), X-ray photoelectron spectroscopy (XPS), low-energy ion scattering spectroscopy (LEISS), a differentially pumped, 5-keV ion gun, several multichannel-array gas dosers connected to precision leak valves, and several metal evaporators. XPS measurements were made by using a dual-anode X-ray source with a Mg anode ($MgK\alpha = 1253.6$ eV).

The Pt crystal had two polished sides, each oriented along the (111) crystal plane and *it was* spot-welded between two tungsten wires (0.8 mm in diameter) wrapped with Pt foil at the spot of contact with the Pt crystal. The crystal could be resistively heated between 300 and 1200 K, as monitored by a chromel–alumel thermocouple that was spot-welded to the side of the crystal.

The procedure used to obtain the Pt–Sn alloys was similar to that described by Paffet and Windham (10). Sn was evaporated onto the Pt(111) surface at 300 K in UHV. This was followed by annealing the Pt(111) crystal to 1000 K for 10 s. To ensure proper alloy formation, both LEED and XPS analyses were done on each surface. Prior to catalytic experiments, the alloy of interest was formed on both sides of the crystal. Special attention was given to ensure that the alloy formed on each of two sides of the crystal was as similar as possible. LEED appeared the same, and XPS revealed differences in the Pt(4f)/Sn(3d) ratio of less than 10% in all cases.

The following procedure was used to obtain a clean Pt(111) surface. The crystal was sputtered by 1-keV Ar^+ ions at room temperature for 1 h and subsequently for 5 min at 1000 K with simultaneous exposure to 1×10^{-7} Torr of oxygen; *it was* then annealed at 1000 K for a few minutes in UHV. Long sputtering times were used to remove all Sn from the near-surface region. After this cleaning procedure, the amount of Sn and carbon on the surface, along with most other common contaminants, was below the XPS detection limit.

The UHV chamber was connected directly through a 4.5-in. gate valve to a stainless-steel batch reactor with a volume of 480 cm^3 that could be pressurized up to 1-atm pressure. The composition of the gas in the reactor cell was analyzed with a Hewlett–Packard 5890 gas chromatograph equipped with a flame ionization detector (FID). An evacuated loop was used to sample the reaction mixture, and an AT-1000 (0.53-mm-diameter, 30-m-long) capillary column was used for product separation.

The Pt crystal was transferred between the UHV analysis chamber and the high-pressure reactor by means of a

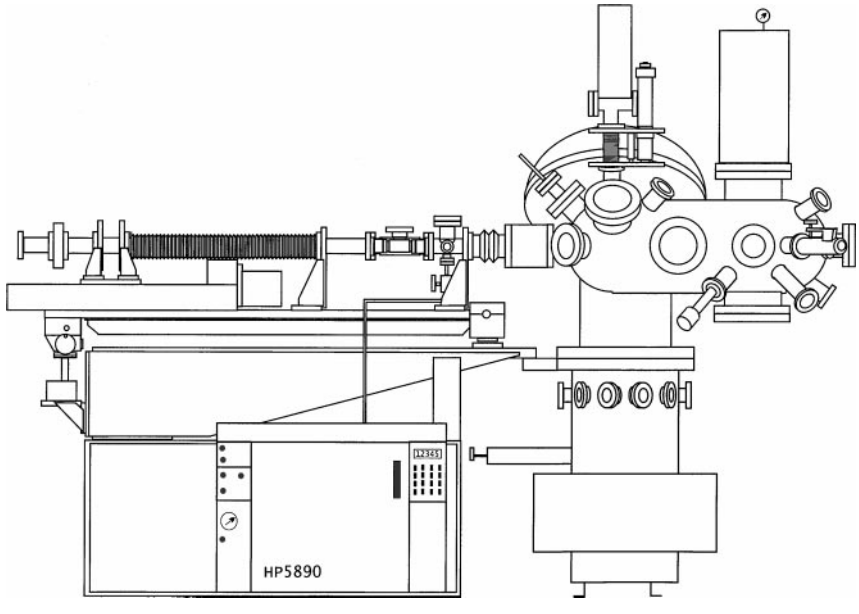

FIG. 1. Schematic drawing of the experimental apparatus.

transfer rod passing through a differentially pumped assembly of sliding seals. The reactor was sealed by the sliding seal at one end and by the gate valve separating the high-pressure cell from the UHV chamber at the other end. The reaction cell could be evacuated with a turbomolecular pump, and it took only a few minutes to bring the cell from a reaction pressure of 5 Torr to a pressure low enough to transfer the sample into the UHV chamber while maintaining a background pressure of 8×10^{-10} Torr. The walls of the reaction cell were heated to 350 K during reaction measurements to decrease the adsorption of crotonaldehyde.

Crotonaldehyde (Aldrich, 99+%) was purified by vacuum distillation prior to use. Hydrogen (Matheson, 99.9999%) was used as supplied. GC analysis of the reaction mixture prior to introduction into the reactor showed 99.99 mol% crotonaldehyde with only a small amount (<0.01 mol%) of light hydrocarbons. We also performed blank experiments to ensure zero catalytic activity (below 1% of the least active catalyst studied) of the reactor in the absence of a catalyst.

Catalytic results are described by selectivity, conversion, and turnover frequencies (TOF) as defined in the following. The selectivity S_i toward a given product was determined as

$$S_i = \frac{n_i}{\sum_i n_i}, \qquad [1]$$

where n_i is the mole fraction of product i in the reaction mixture. The conversion C (mol%) is defined as

$$C = \left(1 - n_c \Big/ \sum n_i\right) \times 100, \qquad [2]$$

where n_c is the mole fraction of crotonaldehyde in the reaction mixture, and $\sum n_i$ is a sum over all components in the reaction mixture. The TOF is defined as the number of crotonaldehyde molecules that undergo hydrogenation per surface atom per second according to

$$\mathrm{TOF} = \frac{V_\mathrm{R} \times P_\mathrm{CH} \times N_\mathrm{A} \times (1 - X_\mathrm{CH})}{R \times T \times t \times \Theta_\mathrm{pt} \times S_\mathrm{pt}}, \qquad [3]$$

where V_R is the reactor volume (3.84×10^{-4} m^3), P_CH is the initial pressure of crotonaldehyde in the reaction mixture (Pa), N_A is Avogadro's number, X_CH is the mol% of crotonaldehyde in the reaction mixture, R is the gas constant, T is the temperature of the reaction mixture (350 K), Θ_Pt is the surface atomic density of Pt(111) (1.505×10^{15} atoms/cm^2), t is the reaction time (seconds), and S is the total surface area of the crystal (1.7 cm^2). No correction was made *a priori* for the reduced number of Pt surface atoms in the alloys.

RESULTS

Catalytic hydrogenation of crotonaldehyde was carried out for a range of temperatures between 350 and 395 K. The temperature of the reactor walls was kept at 350 K to avoid condensation of crotonaldehyde and other reaction products. This temperature determined the lower end of the temperature range. The upper end of the temperature range, 395 K, was determined by the high conversion rates encountered at short reaction times.

The reaction products detected were *n*-butane ($CH_3CH_2CH_2CH_3$), butyraldehyde ($CH_3CH_2CH_2CHO$), *n*-butanol ($CH_3CH_2CH_2CH_2OH$), and crotylalcohol (2-butenol, $CH_3CH{=}CHCH_2OH$). Under all conditions studied for Pt(111) and both Pt–Sn alloys, the main hydrogenation product was butyraldehyde. The amount of the unsaturated alcohol product crotylalcohol was at most 5 mol%.

The activity and selectivity of the $(\sqrt{3} \times \sqrt{3})$R30° and (2×2) Sn/Pt(111) alloys were compared at 365 K using the lowest and highest HC : H_2 ratios (1 : 100 and 1 : 800) that we explored. These two alloys showed similar catalytic performance, with a 10% higher overall activity for the (2×2) Sn/Pt(111) alloy and only a marginal difference in the selectivity. Thus, we chose to present in this paper only the results and conclusions that were specific for the (2×2) Sn/Pt(111) alloy. However, these should also be applicable to the $(\sqrt{3} \times \sqrt{3})$R30° Sn/Pt(111) alloy except for the small differences that were mentioned.

There was no evidence for surface carbon buildup under any conditions on the alloy catalyst. XPS measurements of the carbon coverage taken 20 s after the introduction of the alloy catalyst into the reaction cell showed essentially the same amount of carbon ($\Theta_\mathrm{C} = 0.5$ monolayer (ML)) as that obtained after 30 min of reaction. This was a consequence of the high H_2 : HC ratio that was used, and allowed us to consider that TOF values were not influenced by this factor. The carbon coverage was calibrated with XPS by using ethylene to produce a known coverage of ethylidyne on Pt(111) at 300 K of $\Theta_\mathrm{C} = 0.5$ ML.

Figure 2 shows the composition of the reaction mixture over the (2×2) Sn/Pt(111) alloy catalyst as a function of time. The main product of the reaction was butyraldehyde from hydrogenation of the C=C bond, and only a small portion of crotonaldehyde was converted to the unsaturated alcohol 2-butenol from hydrogenation of the C=O bond. This was a general result for all sets of experimental conditions that were explored.

The influence of temperature on the reaction product yield was monitored at a fixed value of H_2 : HC = 100 and $P_\mathrm{total} = 5$ Torr over a temperature range from 355 to 385 K. These data are shown in Fig. 3. The rates of all monitored processes, i.e., hydrogenation of C=O and C=C functional groups and C=O bond cleavage, increased with increasing temperature. No new products were detected at this temperature range. Using these data, we calculated an apparent activation energy for the hydrogenation of the C=C double bond of $E_\mathrm{app} = 8.6$ kcal/mol at <10% conversion.

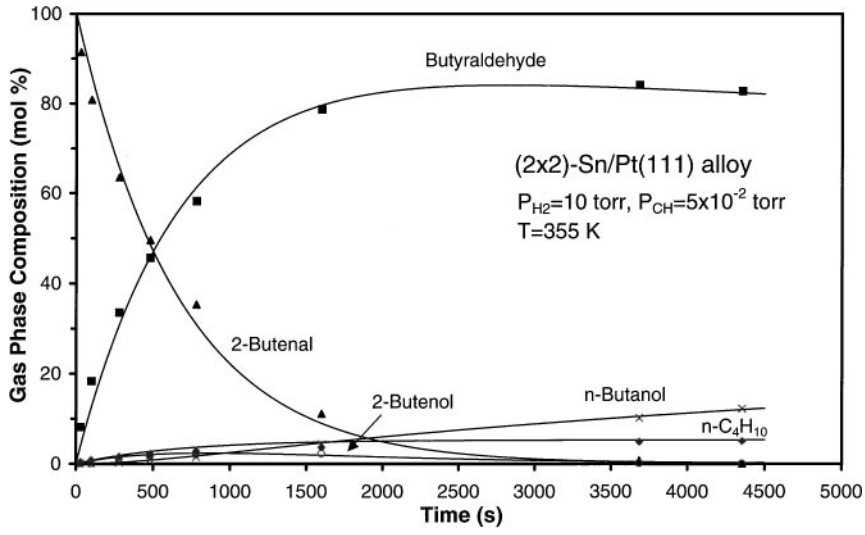

FIG. 2. Composition of the reaction mixture over the (2×2) Sn/Pt(111) surface alloy for the initial reaction conditions: $P_{H_2} = 10$ Torr, $P_{2\text{-butenal}} = 5 \times 10^{-2}$ Torr, and $T = 355$ K.

This was done by assuming that the rate of C=C bond hydrogenation was much higher than that of the C=O bond. This was a reasonable assumption because C=C bond hydrogenation resulting in butyraldehyde formation was the predominant reaction pathway, as shown in Fig. 3.

Arrhenious plots for our results, as well as those for reference data from supported catalysts [1, 11] and another Pt(111) model catalyst, are shown in Fig. 4. To produce these plots for the reference catalysts, we used the hydrogenation rate reported at a specific temperature and extended this through the indicated temperature range using the reported activation energies. Unsupported catalysts displayed higher overall activities than supported catalysts, although one cannot make too much of this difference, because no correction was made for differences in the pressures of crotonaldehyde and hydrogen that were used. The trends on the supported catalysts were similar to those in our data on the unsupported catalysts. Pt–Sn catalysts had higher activity and lower apparent activation engergies than pure Pt catalysts for both supported and unsupported catalysts.

The performance of the (2×2) Sn/Pt(111) model catalyst at 365 K was tested at a crotonaldehyde partial pressure of 5×10^{-2} Torr for several different HC : H_2 ratios: 1 : 100, 1 : 200, 1 : 400, and 1 : 800. Figure 5 shows these results. The rates of formation for all products were positively influenced by H_2 partial pressure except that for *n*-butane which remained nearly constant. The existence of a critical hydrogen partial pressure, above which the reaction rate stops increasing with an increase in H_2 partial pressure, was not encountered in these measurements. This indicates that the rates of all of the reactions, except that of C=O bond cleavage, are proportional to the surface hydrogen concentration which is involved in the limiting steps of these reactions.

Figure 6 quantifies the influence of H_2 partial pressure on the total conversion of crotonaldehyde. As shown in Fig. 6, experiments performed under the same conditions on Pt(111) revealed that the order with respect to H_2 was ~0.5, significantly lower than that for both Pt–Sn alloys which was ~0.9. Because the rate of C=C bond hydrogenation was much higher than that of the C=O bond, this order was mostly related to C=C bond hydrogenation.

Influence of Oxygen Pretreatment

In an attempt to explore the role of metal cations or oxidic species on the selectivity for this catalysis, we tried to produce such species by direct oxidation of the Sn–Pt alloy model catalysts. For these experiments, the (2×2) Sn/Pt(111) alloy was prepared as usual, but *it was* then exposed to 1 Torr O_2 at 600 K for 5 min in the high-pressure cell prior to use as a catalyst. This treatment produced SnO_x species at the surface (12), which we expected would then improve the selectivity toward formation of unsaturated aldehyde based on previous proposals in the supported catalyst literature (13). In addition, we hoped that this experiment would check how exposure of the catalyst to conditions similar to those used industrially for catalytic regeneration might influence catalytic properties.

XPS was used to monitor the amount of oxygen and oxidation states of Sn and Pt before and after oxidation and upon completion of catalytic reactions, as shown in Fig. 7. The 0.8-eV shift of the Sn(3d) peak after the fresh (2×2) Sn/Pt(111) alloy was exposed to oxygen indicated the oxidation of Sn. The total oxygen coverage following this oxidation pretreatment was 1.2 ML. The determination of the Sn oxidation state (II or IV) using XPS is usually regarded as difficult, because nearly identical chemical

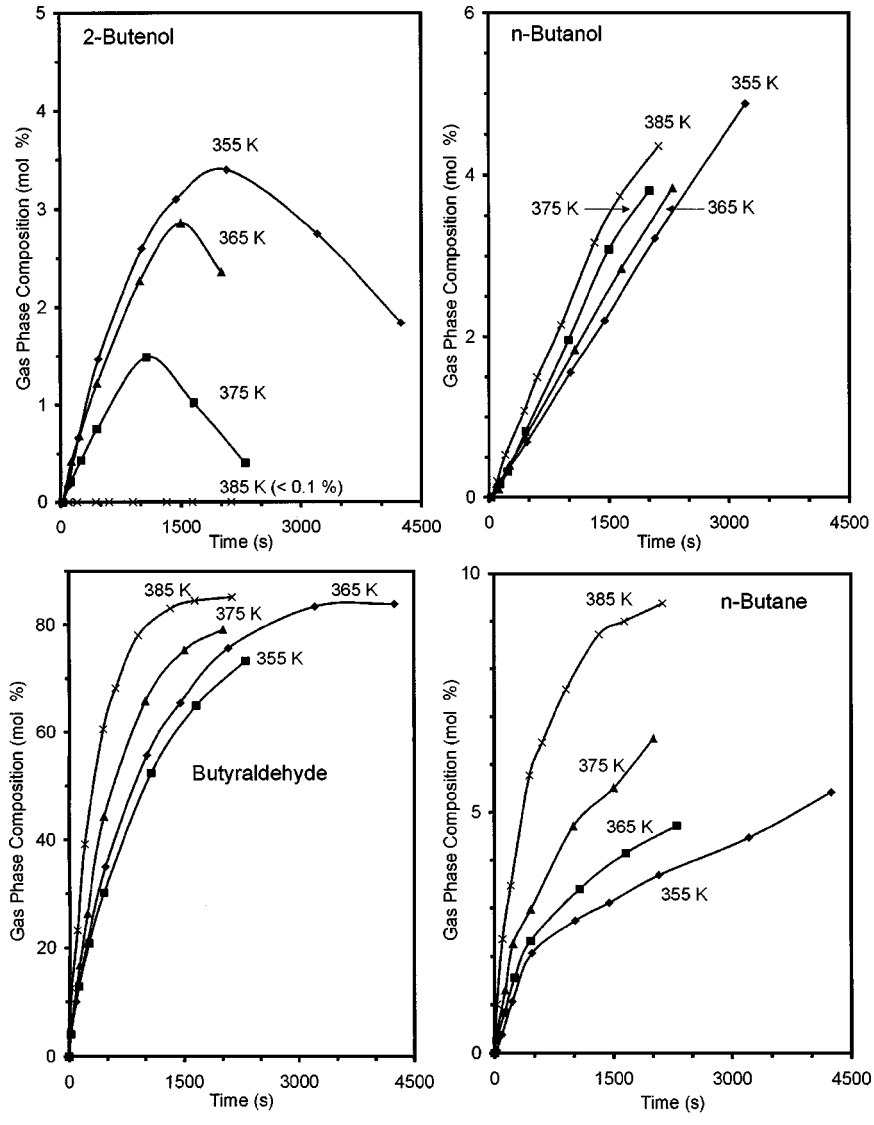

FIG. 3. Composition of the reaction mixture over the (2 × 2) Sn/Pt(111) surface alloy for several temperatures under the following conditions: $P_{H_2} = 5$ Torr and $P_{2\text{-butenal}} = 5 \times 10^{-2}$ Torr.

shifts were reported (14) for those oxidation states. Our XPS results for these surfaces (15) allowed us to exclude formation of SnO_2 (Sn IV) under these conditions, and we assigned the oxidized forms of Sn shown in Fig. 7b to the so-called "quasimetallic" form (16) of Sn (485.6 eV binding energy (BE)) and SnO (486.15 eV BE). The total Sn fraction that was oxidized in one form or the other was equal to 0.9.

Table 1 shows that this oxygen treatment significantly decreased the activity of the (2 × 2) Sn/Pt(111) alloy in subsequent catalytic reactions. The catalytic activity for this sample was lower than that for either the pure Pt(111) or the (2 × 2) Sn/Pt(111) alloy. However, it is evident from Fig. 7c that when the oxidized Pt–Sn alloy was exposed at 365 K to the reaction mixture containing hydrogen, Sn was completely reduced to metallic form. Recent XPS and scanning tunneling microscopy (STM) studies on these same Sn–Pt alloys (17) showed that oxidation takes place by abstraction of Sn from the alloy to form various SnO_x adlayers at the surface. Reduction of this adlayer forms Sn that remains in an adlayer, possibly as Sn rafts, blocking most of the Pt(111) surface. This is because alloying of Sn on Pt(111) requires high temperatures (>600 K) (18). Because Sn itself is not a good catalyst, this results in a sample with low catalytic activity.

We were able to restore the activity of the preoxidized catalyst to that of the normally prepared surface alloy by reduction in 1 Torr H_2 at 600 K for 1 min. This result indictes that oxidation–reduction cycles at 600 K can form an alloy catalyst. Oxygen treatments are commonly used to remove surface carbon deposits, but in the case of Pt–Sn bimetallic catalysts, this treatment also enriches the surface

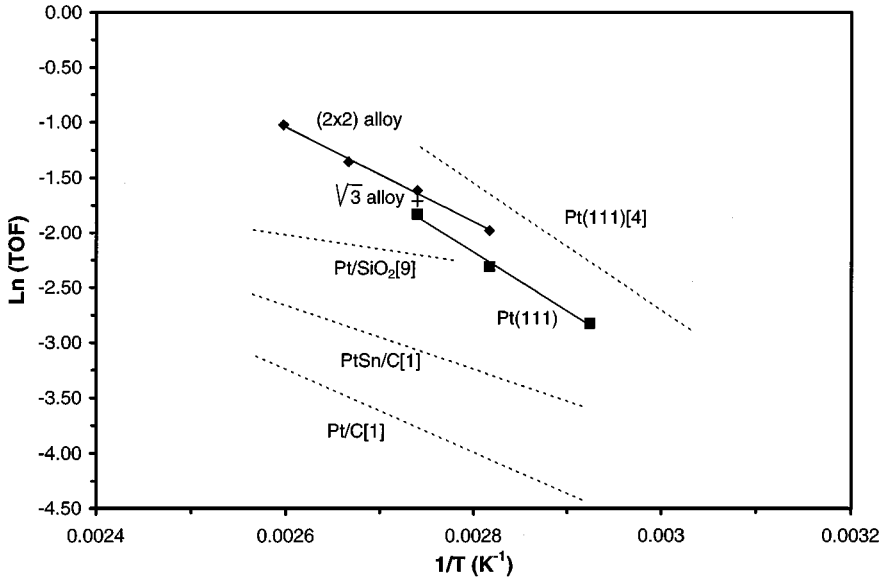

FIG. 4. Arrhenious plots for unsupported Pt(111) and Sn–Pt surface alloys ($P_{H_2} = 5$ Torr and $P_{2\text{-butenal}} = 5 \times 10^{-2}$ Torr) with reference data on supported (1 wt% Pt)/*C*, (1 wt% Pt, 0.25 wt% Sn)/*C*, (0.7 wt% Pt)/SiO_2 and unsupported Pt(111) catalysts.

of the catalyst with Sn. The formation of alloy phases may occur during the subsequent reduction or "activation' stage.

It is useful to compare these results on a preoxidized catalyst to similar experiments performed by Colomna *et al.* (19) on silica and alumina supported PtSn catalysts. They used oxygen pretreatment to elucidate the role of oxidized tin species in the catalytic behavior of $PtSn/SiO_2$ catalysts. They reported reduced activity for oxidized samples compared to those not oxidized, and our observations are similar to theirs. They also reported that the total amount of oxidized tin was 83%, which is close to our value of 90%. In addition, they reported some increase in the activity of these catalysts when the oxidation was performed at elevated temperatures (673 K). This treatment may form ordered tin oxide phases, based on studies done in our group (20), showing that tin oxide overlayers order into well-defined structures on the Pt(111) surface at temperatures above 800 K. This phenomenon may occur on supported catalysts at lower temperatures because of the various metal surface planes exposed, smaller metal particle size, or higher oxygen pressure, and *it may* account for the changes observed in catalytic activity.

DISCUSSION

To obtain kinetic parameters for 2-butenal hydrogenation reactions, we constructed a kinetic model according to the simplified reaction scheme shown in Fig. 8. All reaction pathways that were considered are shown as arrows, with a rate constant for each pathway shown above the arrow. This reaction network can be represented as a system of differential equations; for example,

$$\begin{cases} dC_0/dt = -(k_1 + k_2 + k_3) \times C_0 \\ dC_1/dt = k_1 \times C_0 - k_4 \times C_1 \\ dC_2/dt = k_2 \times C_0 - k_5 \times C_2 \\ dC_3/dt = k_3 \times C_0 \\ dC_4/dt = k_5 \times C_2 + k_4 \times C_1, \end{cases} \quad [4]$$

where C_0, C_1, C_2, C_3, and C_4 are molar concentrations of crotonaldehyde, butyraldehyde, 2-butenol, *n*-butane, and *n*-butanol, respectively. At $t = 0$, $C_0 = 100\%$ and the concentrations of all products were zero.

Within this model, crotonaldehyde can be hydrogenated to butyraldehyde, 2-butenol, and to *n*-butane. The first two products are considered to be intermediates that could be hydrogenated further to form *n*-butanol. The solution to Eq. [4] provides values for these rate constants. This system of equations was solved numerically using the Euler method. The solutions to Eq. [4] at $P_{total} = 10$ Torr, $HC/H_2 = 1:200$, and $T = 365$ K are given as solid lines along with the experimental data points in Fig. 2. All of the rate constants determined in this manner are listed in Table 2. Because the model curves describe the experimental behavior quite well, we believe that the model shown in Fig. 8 is a reasonable approximation.

This kinetic analysis shows that the hydrogenation rate of the C=O bond by the (2×2) Sn/Pt(111) catalyst is 18 times slower than that of the C=C bond. Also, the rate constants for primary (from crotonaldehyde, k_1) and secondary (from 2-butenal, k_5) C=C bond hydrogenation are similar (1.66×10^{-1} versus 1.05×10^{-1}), while rate constants for the primary

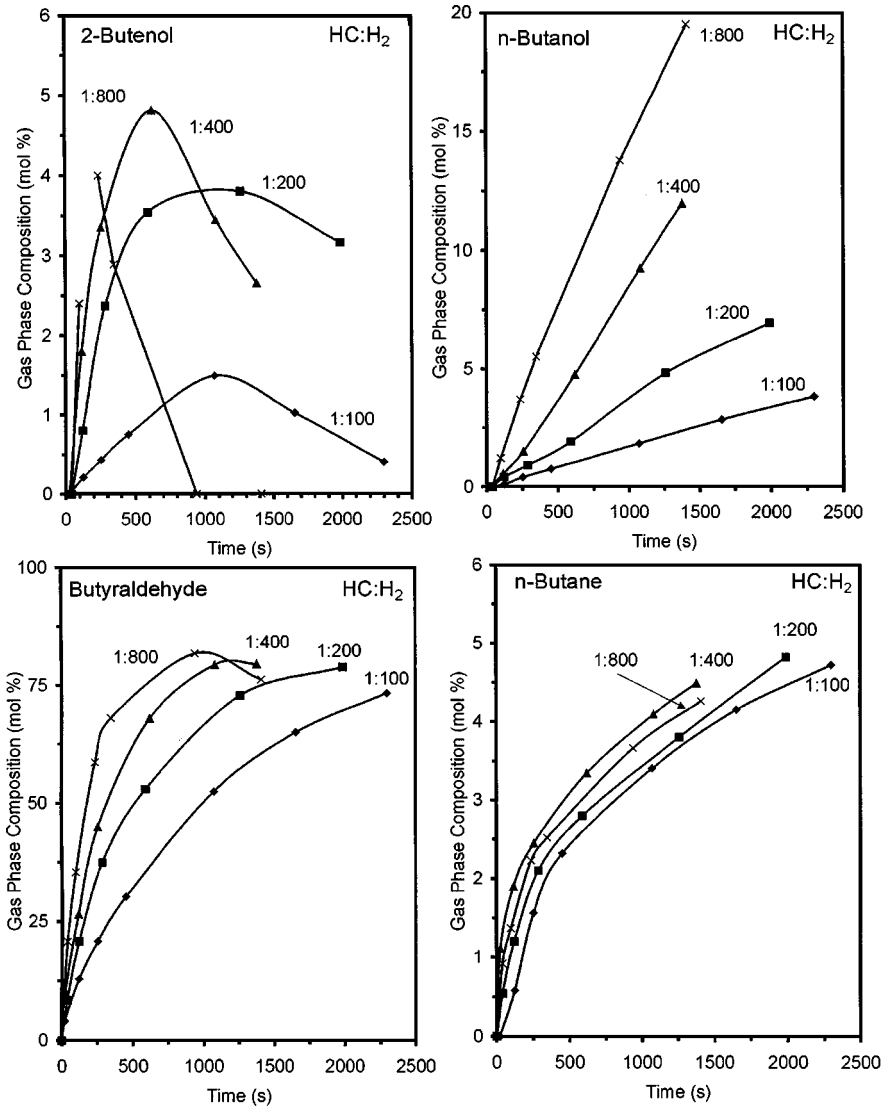

FIG. 5. Influence of the hydrogen pressure on the catalytic activity of the (2 × 2) Sn/Pt(111) surface for the initial conditions: $P_{2\text{-butenal}} = 5 \times 10^{-2}$ Torr and $T = 365$ K.

(k_2) and secondary (k_4) C=O bond hydrogenation differ by a factor of ~3 (9.0×10^{-3} versus 3.0×10^{-3}). The presence of the C=C double bond promotes hydrogenation of the C=O bond in crotonaldehyde over that in butyraldehyde which has no C=C bond. This could result from either an increased residence time for crotonaldehyde or possibly a change in the reaction mechanism due to conjugation between C=C and C=O bonds.

A discussion of the mechanism of crotonaldehyde hydrogenation on Pt–Sn alloys benefits from insights that arise from basic studies of adsorption on Pt and Pt–Sn surfaces. Acrolein and crotonaldehyde adsorption on Pt(111) was studied by Jesus and Zaera (21) by using reflection–absorption infrared spectroscopy (RAIRS) and TPD. To our knowledge, no similar work using these molecules on Pt–Sn alloys has been done yet, but such studies are planned in our laboratory.

TPD studies of crotonaldehyde adsorption on Pt(111) (21) revealed complete decomposition to yield only H_2 and CO desorption products under UHV conditions. No hydrocarbon desorption was observed. This indicates strong, irreversible chemisorption. At submonolayer coverages of crotonaldehyde, the ν(C=O) stretching mode was observed at nearly the same position as that for a condensed phase, multilayer sample, but it had a weak intensity. Jesus and Zaera (21) concluded that the C=O bond was oriented parallel to the surface and interacted only weakly with it. It was concluded that crotonaldehyde was strongly chemisorbed on the Pt(111) surface by nearly complete rehybridization of the C=C bond to give a peak at 1077 cm^{-1} and a formation of two Pt–C σ bonds with the surface, as shown in Fig. 9a. Semiempirical extended Huckel calculations support this picture (22). A limiting case for di-σ-bonded adsorption through rehybridization of the C=O bond is shown in

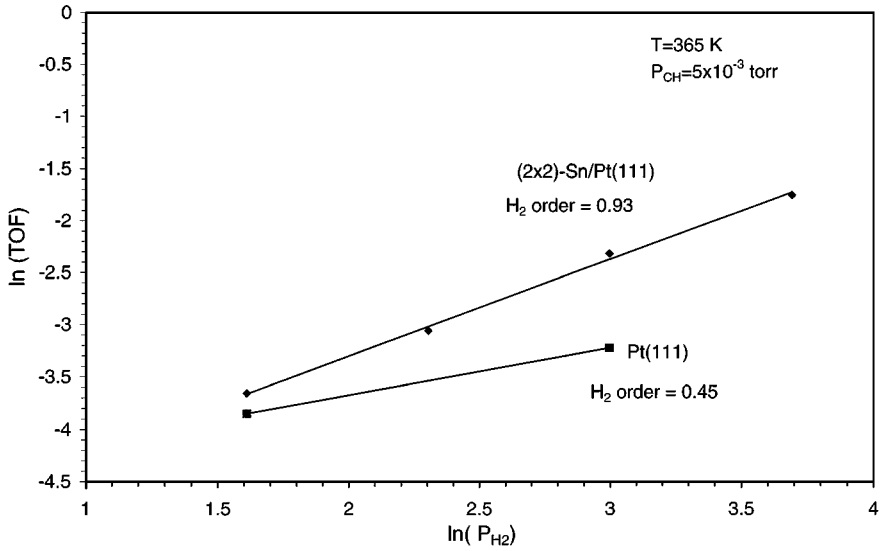

FIG. 6. Reaction order plot for the (2 × 2) Sn/Pt(111) surface alloy and Pt(111) surfaces for $P_{2\text{-butenal}} = 5 \times 10^{-2}$ Torr and $T = 365$ K.

Fig. 9b. However, carbonyl functional groups usually interact weakly with Pt surfaces by forming a dative bond via the oxygen atom (23). We should not exclude a possible role for π-bonded crotonaldehyde molecules in which the C═C and C═O double bonds are conjugated and oriented in the plane parallel to the surface as shown in Fig. 9c.

The adsorption energy for crotonaldehyde on these surfaces may help to explain the different dependencies on hydrogen pressure. We observed a positive order with respect to hydrogen pressure on all surfaces, with values of 0.9 on the Pt–Sn alloys and 0.5 on Pt(111). For hydrogenation of the C═C bond, the rate should depend on both surface hydrogen concentration and crotonaldehyde adsorption energy. Previous studies of olefins (24) lead us to expect that crotonaldehyde is more weakly bound to the alloys than to Pt(111), and thus H_2 pressure should have a more important effect on the rate on the alloys than on the Pt(111) surface. If breaking the Pt–C bond is involved in the rate-determining

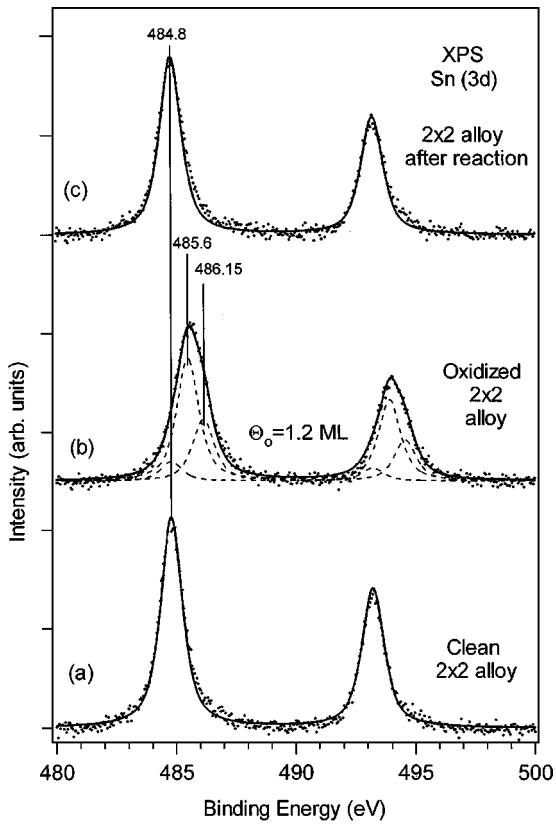

FIG. 7. Sn(3d) peaks in XPS for alloys before (a) and after (b) oxidation of the (2 × 2) Sn/Pt(111) alloy and after (c) the oxidized alloy was used as a catalyst.

TABLE 1

Hydrogenation Activity of Model Catalysts for $P_{H_2}/P_{HC} = 100$, $P_{H_2} = 5$ Torr, and $T = 365$ K

Catalyst	Sn coverage	E_a(app) (kcal/mol)	Overall hydrogenation activity (TOF) s^{-1}
Pt(111)	0	10.8 (11.0 (4))	0.13 (0.31 × (4))
(2 × 2) Sn/Pt(111) alloy	0.25	8.6	0.21
($\sqrt{3} \times \sqrt{3}$)R30° Sn/Pt(111) alloy	0.33		0.18
(2 × 2) alloy + oxidation in 1 Torr O_2 at 600 K for 5 min			0.05
Oxidized (2 × 2) alloy + reduction in 1 Torr of H_2 at 600 K for 1 min	0.25		0.25

Note. Measured at $P = 3$ Pa, $T = 330$ K. The original TOF value of 5.6×10^{-2} s^{-1} was extrapolated to 365 K by using the reported activation energy of 46 kJ/mol (4).

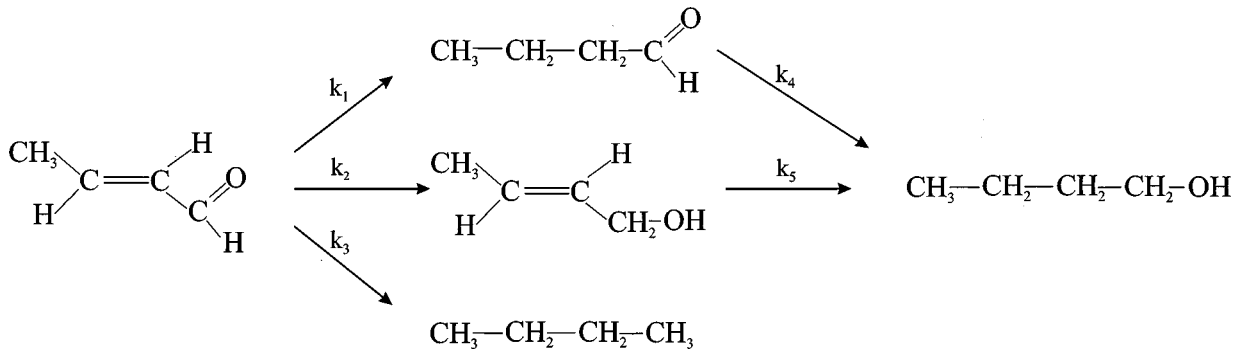

FIG. 8. Reaction network for 2-butenal hydrogenation.

step, this could also explain the lower apparent activation energies on the alloys compared to those on Pt(111), which are 8.6 kcal/mol for the two Pt–Sn alloys and 10.8 kcal/mol for Pt(111).

The full hydrogenation of 2-butenal to *n*-butane proceeds via the cleavage of the C–OH bond, as shown in Fig. 9d. This hydrogenation pathway, as we mentioned when discussing Fig. 5, is the only one which does not depend on the hydrogen partial pressure. The overall process for producing butane includes a number of elementary steps such as C–OH bond cleavage, hydrogenation of surface intermediates, and desorption of the butane and water products. Surface science studies showed that desorption of butane (25) and water (26) was very fast under catalytic conditions. Among the remaining steps, only C–OH cleavage does not directly involve hydrogen, and we can conclude that this must be the limiting step for the full hydrogenation process. The fact that hydrogenation of alkyl groups is not rate limiting is consistent with expectations based on observations that such reactions are facile on Pt(111) and these Pt–Sn alloys.

If we assume that C–OH cleavage is the limiting step for *n*-butane formation, then we can use the rate of *n*-butane formation versus temperature data to calculate an activation energy for C–OH bond cleavage. We determine a value of 11.2 kcal/mol on the (2×2) alloy. If the alloys follow the same trend as that on Pt(111), where the activation energies for C=C and C=O hydrogenation are very close (4), an increase in temperature will favor *n*-butane production.

Another feature observed in Figs. 3 and 5 was that there were two distinct regimes in the rate of *n*-butane production; i.e., all curves for the *n*-butane yield clearly displayed a "break" or change in slope as a function of time. The first regime was observed at low conversion when the most abundant component in the reaction mixture was crotonaldehyde which could be characterized by a fairly high rate of *n*-butane production. The second regime was observed at higher conversions and had a lower rate primarily because *n*-butane formation under these conditions occurred from butyraldehyde. This interpretation implies that adsorbed species containing a C=C double bond are more susceptible to C–OH cleavage.

The main difference in crotonaldehyde hydrogenation on Pt–Sn surface alloy catalysts compared to that on Pt(111) is an increased activity for all hydrogenation reactions that were monitored. Both C=O and C=C hydrogenation reactions were promoted to an equal extent. One factor influencing this increased activity is a change in the electronic state of Pt that is induced by alloying with Sn. This change influences the bond strength between the adsorbed species and the surface. It was reported that such hydrogenation reactions occured faster on surfaces with decreased electron density (27). While no significant shifts occur in the Pt core levels due to formation of the surface alloys (28), there is a reduction in the density of states at E_F that is revealed in ultraviolet photoelectron spectroscopy (29). Furthermore, recent scanning tunneling microscopy studies (30) reported an "electronic contrast" for Pt atoms depending on the number of Sn neighbors bonded to a Pt atom, and this gives direct evidence for charge transfer from Pt to Sn to reduce the electron density at Pt sites. This then presents a consistent picture for explaining our catalytic results. Second, the ensemble size of contiguous reactive Pt atoms at the surface is changed by alloying with Sn. However, since hydrogenation reactions do not require large ensembles, the reduced ensemble size for the Pt–Sn alloys should not influence this particular type of reaction.

TABLE 2

Rate Constants for the Different Reaction Pathways Shown in Fig. 7 on the (2×2) Sn/Pt(111) Alloy Catalyst for $P_{H_2}/P_{HC} = 200$, $P_{H_2} = 10$ Torr, and $T = 365$ K

Rate constant	TOF (s^{-1})	E_a(app) (kcal/mol)
k_1, *n*-Butenal	0.166	8.6
k_2, 2-Butenol	0.009	
k_3, *n*-Butane	0.010	11.2
k_4, *n*-Butanol	0.003	
k_5, *n*-Butanol	0.105	
Overall TOF	0.29	

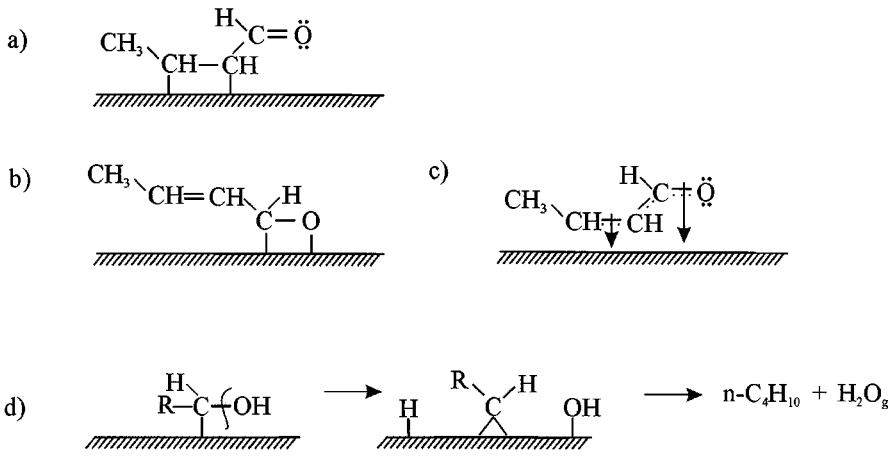

FIG. 9. Reactive species expected to be present on the metal surface during hydrogenation of crotonaldehyde and possible reaction mechanisms.

It is useful to compare our newly obtained results for well-defined, unsupported Pt–Sn alloys to results from Pt and Pt–Sn catalysts supported on carbon black (1). An increase in the overall activity and a decrease in the apparent activation energy were observed on both unsupported and supported Pt–Sn catalysts with respect to Pt catalysts. The primary difference was that the TOF values reported for the supported catalysts (1) were about 10 times lower than those obtained in this study. Furthermore, the supported catalyst with a 25% Sn loading had twice the overall activity of a pure Pt supported catalyst, and we also observed that the (2×2) Sn/Pt(111) catalyst, which had 25% Sn atoms in the surface layer, had twice the overall activity of the Pt(111) catalyst. However, increasing the Sn coverage further to 33% for the $(\sqrt{3} \times \sqrt{3})$R30° Sn/Pt(111) alloy resulted in a decrease of 10% in the TOF, while for supported catalysts, the highest activity was observed for a catalyst with 50% Sn loading. We also did not observe a significant change in selectivity between pure Pt and Pt–Sn model catalysts, whereas supported Pt–Sn catalysts exhibited improved selectivity for C=O bond hydrogenation with increased Sn loading.

These differences are revealing about the origin of the improved performance of the supported catalysts because the unsupported catalysts are quite different, and more defined, from the supported catalysts. One difference is that the morphology of the supported catalyst is obviously different from that of the model catalysts. The influence of the support is an important factor that could affect the metal particle size, shape, and electron density, and change adsorption energies, geometries, and reaction mechanisms. "Spillover" effects that lead to communication between adsorbed species on the support and metal particles can also occur. Changing the Sn loading might and should affect all of these interactions. Also, high Sn loadings may also result in larger amounts of unreduced Sn present in the catalyst that are not incorporated into Pt–Sn alloy phases. Our unsupported catalysts reveal the importance of Pt–Sn phases of specific composition and structure, thus defining the role that these phases play in supported catalysts.

As mentioned earlier, one of the major factors thought to influence hydrogenation selectivity of unsaturated aldehydes is a higher preference for adsorption via the C=O bond versus the C=C bond. In the model proposed by Marinelli and Ponec (31), an important factor facilitating adsorption via the C=O bond was the presence of metal cations present in oxidic phases at the catalyst surface. These species could be produced by partial oxidation of the primary catalytic metal component, e.g., Pt (1), during catalyst pretreatment and by oxidation of the more electropositive promoters such as Sn or Fe. Based on similar activities of reduced Pt–Sn and Pt–SnO_x catalysts, it was concluded that the promotion effect was a result of cations which survived reduction or were formed upon initial contact with the aldehyde (32). The latter possibility was supported by the observation that the activity increased when CO pulses were added to the reaction mixture (31). Our results on the reduced Pt–Sn alloy model catalyst show that alloy phases alone do not lead to an increase in selectivity. To this extent, our results are consistent with the explanation of Marinelli and Ponec (31) concerning supported catalysts.

The results after preoxidation of the (2×2) Sn/Pt(111) alloy differ significantly from those obtained previously for freshly prepared Pt–Sn catalysts supported on carbon black (1) in which most of the Sn and a significant amount of the Pt were oxidized. While we found complete reduction of SnO_x on our model catalysts, only 11% of the total Sn loading was reduced on the supported catalyst even after thermal treatment in hydrogen (12 h in H_2 flow at 760 Torr at 623 K). Carbon black is an inert support, interacting only weakly with supported metal particles; thus, the observed difference in the extent of Sn reduction must be a result of the nature of the phase and domain size of SnO_x formed and/or of the chemical state of Pt. On carbon black some of the supported Pt prior to reduction was found to be in oxidic form (i.e., Pt (II)). We did not observe any changes in

the Pt(4f) XPS peak position after our oxygen treatment, indicating that oxidation under our conditions preserved Pt in a metallic state. This decreased the thermal stability of SnO_x species (33) and increased their reducibility by H_2.

Further work is needed to clarify the influence of oxidic species on selectivity. Because SnO_x species formed by oxidation of Pt–Sn alloys are immediately reduced, we plan work in the future with admetals forming more stable oxides. The change from Sn to a more electropositive metal such as Fe should increase the stability of oxidic species and allow them to withstand reaction conditions that completely reduce SnO_x.

CONCLUSION

Gas-phase hydrogenation of crotonaldehyde over Pt(111) and two ordered surface alloys, a (2×2) Sn/Pt(111) and a $(\sqrt{3} \times \sqrt{3})$R30° Sn/Pt(111) structure, was studied at a temperature range from 355 to 395 K, a H_2 pressure range from 5 to 40 Torr, and a HC/H_2 ratio range from 1 : 100 to 1 : 800. The Pt–Sn alloy catalysts displayed about twice the activity of the Pt(111) model catalyst, with the activity of the (2×2) Sn/Pt(111) about 10% higher than that for the $(\sqrt{3} \times \sqrt{3})$R30° Sn/Pt(111) alloy. However, the selectivity observed on all of the model catalysts was similar, with butyraldehyde formed as the main product. We conclude that the improvement in selectivity toward formation of the unsaturated alcohol that has often been reported for Pt–Sn catalysts versus supported pure Pt catalysts cannot be solely due to Pt–Sn alloy formation. Pt–Sn alloys that were preoxidized at 600 K in O_2 had a lower catalytic activity than either of the Pt–Sn surface alloys or the Pt(111) surface. We propose that this results from dealloying Sn to form the SnO_x adlayer during oxidation followed by reduction of the oxidic Sn to an inactive metallic Sn adlayer during low-temperature catalytic reaction. The catalytic activity of the preoxidized alloys can be restored to that for the as-prepared alloys by H_2 reduction at a temperature exceeding 600 K.

ACKNOWLEDGMENT

This work was supported by the Division of Chemical Sciences, Office of Basic Energy Sciences, U.S. Department of Energy.

REFERENCES

1. Coloma, F., Sepulveda-Escribano, A., Fierro, J. L. G., and Rodriguez-Reinoso, F., *Appl. Cat. A Gen.* **136**, 231 (1996).
2. Szanyi, J., Anderson, S., and Paffet, M. T., *J. Catal.* **149**, 438 (1994).
3. Bodke, A. S., Olschki, D. A., Schmidt, L. D., and Ranzi, E., *Science* **285**, 712 (1999).
4. Beccat, P., Bertolini, J. C., Gauthier, Y., Massardier, J., and Ruiz, P., *J. Catal.* **126**, 451 (1990).
5. Balakrishnan, K., and Schwank, J., *J. Catal.* **68**, 42 (1981).
6. Bond, G. C., "Catalysis of Metals." Academic Press, London, 1962.
7. Rylander, P. N., *in* "Catalytic Hydrogenation in Organic Synthesis," p. 72. Academic Press, New York, 1979.
8. Ponec, V., *Appl. Catal. A Gen.* **149**, 27 (1997).
9. Marinelly, T. B. L. W., Vleeming, J. H., and Ponec, V., *in* "Proceedings, 10th International Congress on Catalysis, Budapest, 1992" (L. Guczi, F. Solymosi, and P. Tetenyi, Eds.), Vol. 2, p. 1211. Akadémiai Kiadó, Budapest, 1993.
10. Paffet, M. T., and Windham, R. G., *Surf. Sci.* **34**, 208 (1989).
11. Vannice, M. A., and Sen, B., *J. Catal.* **115**, 65 (1989).
12. Batzill, M., Beck, D. E., and Koel, B. E., *Appl. Phys. Lett.* **78**, 2766 (2001).
13. Gallezot, P., and Richard, D., *Catal. Rev.* **40**, 81 (1998).
14. Weaver, J. F., Campbell, T. J., Hoflund, G. B., and Salaita, G. N., *J. Electron. Spectrosc. Relat. Phenom.* **106**, 81 (2000).
15. Jerdev, D., and Koel, B. E., submitted.
16. Rotermund, H. H., Penka, V., DeLouise, L. A., and Brundle, C. R., *J. Vac. Sci. Technol.* **5**, 1132 (1987).
17. Batzill, M., Beck, D., and Koel, B. E., submitted.
18. Paffet, M. T., and Windham, R. G., *Surf. Sci.* **208**, 34 (1989).
19. Colomna, F., Llorca, J., Narcis, H., Ramirez de la Piscina, P., Rodrigez-Reinoso, F., and Sepulvedo-Escibano, A., *Phys. Chem. Chem. Phys.* **2**, 3063 (2000).
20. Batzill, M., Beck, D. E., Jerdev, D., and Koel, B. E., *J. Vac. Sci.* **19**, 1037 (2001).
21. Jesus, J. C., and Zaera, F., *Surf. Sci.* **99**, 430 (1999).
22. Delbecq, F., and Sautet, P., *J. Catal.* **152**, 217 (1995).
23. Marinelli, T. B. L. W., Nabuurs, S., and Ponec, V., *J. Catal.* **151**, 431 (1995).
24. Tsai, Y. L., Chen, X., and Koel, B. E., *Surf. Sci.* **358**, 37 (1997).
25. Salmeron, M., and Somorjai, G. A., *J. Phys. Chem.* **85**, 3835 (1981).
26. Wagner, F. T., and Moylan, T. E., *Surf. Sci.* **191**, 121 (1987).
27. Blackmond, D. G., Oukaci, R., Blank, B., and Gallezot, P., *J. Catal.* **131**, 401 (1991).
28. Paffett, M. T., and Windham, R. G., *Surf. Sci.* **208**, 34 (1989).
29. Paffett, M. T., Gebhard, S. C., Windham, R. G., and Koel, B. E., *Surf. Sci.* **223**, 449 (1989).
30. Batzill, M., Beck, D. E., and Koel, B. E., *Surf. Sci.* **466**, L821 (2000).
31. Marinelli, T. B. L. W., and Ponec, V., *J. Catal.* **156**, 51 (1995).
32. Marinelli, T. B. L. W., Nabuurs, S., and Ponec, V., *J. Catal.* **151**, 431 (1995).
33. Saliba, N. A., Tsai, Y. L., and Koel, B. E., *J. Chem. Phys.* **103**, 1532 (1999).